# Complex Surface Chemistry of 4-Mercaptopyridine Self–Assembled Monolayers on Au(111)

7 **AUTHORS**, INCLUDING:

**Emiliano Cortés**
Imperial College London
**22** PUBLICATIONS **312** CITATIONS

SEE PROFILE

**Pilar Carro**
Universidad de La Laguna
**56** PUBLICATIONS **1,181** CITATIONS

SEE PROFILE

**G. Benitez**
National Scientific and Technical Research Co…
**75** PUBLICATIONS **1,578** CITATIONS

SEE PROFILE

**Roberto C Salvarezza**
National Scientific and Technical Research Co…
**342** PUBLICATIONS **6,411** CITATIONS

SEE PROFILE

# Complex Surface Chemistry of 4-Mercaptopyridine Self-Assembled Monolayers on Au(111)

E. A. Ramírez,[†] E. Cortés,[†] A. A. Rubert,*,[†] P. Carro,[‡] G. Benítez,[†] M. E. Vela,[†] and R. C. Salvarezza[†]

[†]Instituto de Investigaciones Fisicoquímicas Teóricas y Aplicadas (INIFTA), Facultad de Ciencias Exactas, Universidad Nacional de La Plata − CONICET, Sucursal 4 Casilla de Correo 16, (1900) La Plata, Argentina

[‡]Departamento de Química Física, Instituto de Materiales y Nanotecnología, Universidad de La Laguna, Tenerife, Spain

**ABSTRACT:** The adsorption of 4-mercaptopyridine on Au(111) from aqueous or ethanolic solutions is studied by different surface characterization techniques and density functional theory calculations (DFT) including van der Waals interactions. X-ray photoelectron spectroscopy and electrochemical data indicate that self-assembly from 4-mercaptopyridine-containing aqueous 0.1 M NaOH solutions for short immersion times (few minutes) results in a 4-mercaptopyridine (PyS) self-assembled monolayer (SAM) with surface coverage 0.2. Scanning tunneling microscopy images show an island-covered Au surface. The increase in the immersion time from minutes to hours results in a complete SAM degradation yielding adsorbed sulfur and a heavily pitted Au surface. Adsorbed sulfur is also the main product when the self-assembly process is made in ethanolic solutions irrespective of the immersion time. We demonstrate for the first time that a surface reaction is involved in PyS SAM decomposition in ethanol, a surface process not favored in water. DFT calculations suggest that the surface reaction takes place via disulfide formation driven by the higher stability of the S−Au(111) system. Other reactions that contribute to sulfidization are also detected and discussed.
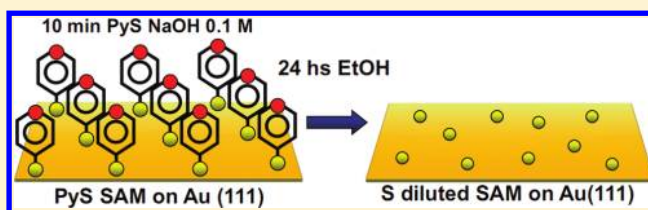
## ■ INTRODUCTION

Self-assembled monolayers (SAMs) of thiols on Au have attracted considerable attention because they have been employed as passive or active elements in the fabrication of molecular systems and devices through the bottom-up approach in the wide field of nanotechnology.[1−5] The initial stage of alkanethiol chemisorption on Au(111) involves the formation of lying-down phases with the molecules parallel to the substrate. A transition from the lying-down to a standing-up configuration (tilt angle ≈30° with respect to the substrate normal) takes place by increasing the surface coverage in both gas phase and liquid phase preparation leading to the formation of the dense and stable $(\sqrt{3} \times \sqrt{3})$-$R30°$ and c(4 × 2) lattices. They exhibit thiol surface coverage $\theta = 0.33$ and nearest-neighbor thiol−thiol distances $d \approx 0.5$ nm.[3,6] Similar surface structures are formed in SAMs of aromatic thiols.[7] Aliphatic and aromatic thiol are chemisorbed on Au by a strong thiolate−Au bond (40−50 kcal mol$^{-1}$) characterized by a S 2p X-ray photoelectron spectroscopy (XPS) signal at ≈162 eV,[6] i.e., a lower binding energy than that of bulk sulfur (≈164 eV).[8]

The chemisorption process induces strong changes in the substrate with the formation of vacancy islands of monatomic depth in the case of aliphatic thiols and of gold islands in the case of some aromatic thiols as observed by scanning tunneling microscopy (STM).[9,10]

In the case of small aliphatic or aromatic thiol molecules more diluted lattices ($\theta < 0.33$) have also been found,[10−12] and in some cases, for instance, methanethiol SAMs formed from dimethyl disulfide and cysteamine SAMs,[13,14] the presence of

significant amounts of coadsorbed atomic sulfur (S) has been reported depending on the experimental conditions for self-assembly. It has been proposed that the presence of S arises either from a small amount of contamination in the thiols[15] or from the C−S bond scission at the Au(111) surface.[14] Among these short thiol molecules 4-mercaptopyridine (PySH) on Au(111) is a very interesting case. In fact, SAMs of this molecule have been widely used to anchor different metallic cations for SAM metallization[16,17] and sensing[18,19] or for building devices for molecular electronics,[20] as a linker of biomolecules that facilitate heterogeneous charge transfer reactions,[21] and also for surface-enhanced Raman spectroscopy (SERS) studies.[22] In most cases 7 × $\sqrt{3}$ or 5 × $\sqrt{3}$ lattices ($\theta \approx 0.2$) have been imaged by STM in electrolyte solutions instead of the typical $(\sqrt{3} \times \sqrt{3})$-$R30°$ and c(4 × 2) lattices found for aliphatic and aromatic thiols ($\theta \approx 0.33$). DFT calculations have confirmed the stability of the (7 × $\sqrt{3}$) structure, but the experimentally observed (5 × $\sqrt{3}$) structure does not appear to be a thermodynamically stable structure.[23] These calculations also predict the formation of the $(\sqrt{3} \times \sqrt{3})$-$R30°$ chemisorbed PySH (from here denoted as PyS) at high chemical potentials although this surface structure has not been experimentally observed yet. A more diluted (12 × $\sqrt{3}$) lattice has been experimentally observed by STM in alkaline media although it was imaged along PyS desorption.[24] On the

other hand, STM images in acid media have suggested that the PyS species are dimerized at the sulfur position to form a disulfide.[24,25]

In addition to the complex surface structure possible side reactions in PySH solutions yielding sulfide and disulfide species introduce uncertainty in the chemical composition and stability of the PyS SAMs.[26] In fact, electrochemical and spectroscopic evidence have been obtained indicating that PySH and 4,4′-dipyridyl disulfide (Py−S−S′−Py) decompose spontaneously into atomic and oligomeric S species.[27] However, this process was not observed for 2-mercaptopyridine so that the authors were not able to explain the mechanism involved in sulfidization. The solvent seems to play some role in the self-assembly of PySH as a large increase in the vacancy islands formed upon thiol adsorption has been observed when the process is made in ethanolic solutions.[28] Also in this case no explanation for this observation has been advanced. The extensive etching of the Au surface in ethanol has been later explained by the formation of soluble PyS−Au(I)−SPy species, a process that does not require the formation of thiolate−Au bonds.[29] Therefore, elucidation of the chemistry of the PyS SAMs is crucial if they have to be used as active or passive elements in sensors, biosensors, or molecular electronics devices.

In this work we have performed an experimental study of PySH adsorption on the Au(111) surface in order to clarify relevant unsolved issues such as the observation of sulfur, disulfide, and thiolate adlayers, depending on the solvent or electrolyte pH, the mechanism of sulfidization, and the strong dependence of surface topography with the solvent. Our experimental and theoretical results shed light on all these problems, revealing the complexity of the surface chemistry of this system.

## ■ EXPERIMENTAL SECTION

**Materials.** 4-Mercaptopyridine (PySH) (Aldrich, 95%), hexane-thiol (HT) (Aldrich, 95%) used for control experiments, NaOH (Sigma, 98.6%), and absolute ethanol (Carlo Erba, 99.8%) were used as received. Evaporated Au films on glass with (111) preferred orientation (Arrandees, Germany) were used as substrates. After soft annealing for 5 min with a hydrogen flame these Au substrates exhibit atomically smooth (111) terraces separated by monatomic steps in height, as revealed by scanning tunneling microscopy (STM).

**PySH Self-Assembly.** PyS SAMs were formed on the Au(111) substrates by immersion of the clean substrates in previously deaerated 1 mM solutions in aqueous 0.1 M NaOH or ethanol for 10 min or 24 h. After incubation the samples were rinsed with the solvent and dried with N$_2$. Then they were immediately (i) placed in the electrochemical cell for voltammetry, (ii) imaged in air by STM, or (iii) placed in the UHV chamber for X-ray photoelectron spectroscopy (XPS) analysis.

**Electrochemical Measurements.** Reductive desorption curves RDC were performed with a TEQ potentiostat with digital data acquisition. The thiol-modified Au(111) substrate (working electrode) was mounted in a conventional three-electrode glass cell using a Pt large area foil as counter and a saturated calomel electrode (SCE) as reference electrodes. The 0.1 M NaOH aqueous solutions were prepared by using deionized H$_2$O (18 Mohm cm) from a Milli-Q purification system (Millipore Products, Bedford) and were degassed with purified nitrogen prior to the experiments.

Thiol reductive electrodesorption was performed by scanning the potential from −0.2 to −1.4 at 0.05 V s$^{-1}$ in the 0.1 M NaOH solution at room temperature. In each case the charge density involved in the reductive desorption (calculated by integration of the peak area and taking into account the electrode real area from the gold oxide reduction peak) was taken as an indication of the surface coverage by the SAM. Results are an average of more than five measurements.

**X-ray Photoelectron Spectroscopy.** XPS measurements were performed using a Mg Kα source (XR50, Specs GmbH) and a hemispherical electron energy analyzer (PHOIBOS 100, Specs GmbH) operating at 10 eV pass energy. A two-point calibration of the energy scale was performed using sputtered cleaned gold (Au 4f$_{7/2}$, binding energy = 84.00 eV) and copper (Cu 2p$_{3/2}$, binding energy = 932.67 eV) samples. C 1s at 285 eV was used as reference when required. Spectra were analyzed with CasaXPS v2.3.14 and XPS Peak 4.1 software packages. A Shirley-type background was used to each spectrum region.

In order to set the quality of the SAM, the fitting of the S 2p (Au 4f) peaks was carried out by using a spin−orbit splitting of 1.2 eV (3.65 eV) and a branching ratio of 0.5 (0.75). The surface coverage by the thiol molecules was estimated using the ratio measurement between the areas of S 2p region at 162.2−162.3 eV and the corresponding Au 4f signal for each sample, corrected by the relative sensitivity factor (RSF) of the elements. The S 2p/Au 4f area signal ratio was converted to coverage using as a reference the value corresponding to hexanethiol SAM which has a surface coverage $\theta_{SAM}$ = 0.33. This procedure has been used previously to estimate thiol SAMs coverage by XPS measurements.[6,30,31] The electron attenuation factor introduced by the presence of the organic layer is similar for S and Au, and the electron attenuation factor for Au due to S atom contribution is negligible. On the other hand, the fitting N 1s region required at least three peaks with equal FWHM constrains to be adjusted.

**STM Characterization.** Scanning tunneling microscopy (STM) images were obtained in air using a Nanoscope IIIa microscope from Veeco Instruments (Santa Barbara, CA). Mechanically cut Pt−Ir tips were used. Typical tunneling currents and bias voltages for imaging were 500 pA−1 nA and 300−500 mV, respectively.

**Density Functional Theory Calculations.** We have performed *ab initio* periodic DFT calculations using plane-wave pseudopotential. The exchange-correlation potential was described by means of the generalized gradient approach (GGA) with the Perdew−Wang (PW91)[32] implementation. The one-electron wave functions have been expanded on a plane-wave basis set with a cutoff of 520 eV for the kinetic energy. The projector augmented wave (PAW) method[33,34] as implemented by Kresse and Joubert[35] has been employed to describe the effect of the inner cores of the atoms on the valence electrons. The energy minimization (electronic density relaxation) for a given nuclear configuration was carried out using a Davidson block iteration scheme. The dipole correction was applied to minimize polarization effects caused by asymmetry of the slabs. All calculations have been carried out using the VASP 5.2.11 package.[35,36] The long-range dispersion corrections have been taken into account within a DFT-D2 approach of Grimme[37] as implemented in that version of VASP. Since the gold atom is not described in the original paper of Grimme, we have used for the dispersion coefficient $C_6$ and the van der Waals (vdW) radius $R_0$ 40.62 J nm$^6$/mol and 1.772 Å, respectively.[38,39]

The Au(111) surface was modeled by a periodic slab composed of five metal layers and a vacuum of ∼12 Å. Adsorption occurs only on one side of the slab. During the geometry optimization the two bottom layers were kept fixed at their optimized bulk truncated geometry for the Au(111) surface. The three outermost atomic metal layers, as well as the atomic coordinates of the adsorbed species, were allowed to relax without further constraints. The atomic positions were relaxed until the force on the unconstrained atoms was less than 0.03 eV/Å.

The unit cells employed were (7 × $\sqrt{3}$), ($\sqrt{3}$ × $\sqrt{3}$)-R30° of the Au(111) surface that contain three and one PyS or one S, respectively. It should be noted that the (7 × $\sqrt{3}$) PyS structure has been proposed to be the most stable configuration for chemisorbed PyS.[23] In this structure there are three inequivalent PyS species per surface unit cell. The Brillouin zone sampling was carried out according to the Monkhorst-Pack[40] scheme with (3 × 9 × 1) and (9 × 9 × 1) dense k-points meshes depending on the unit cell. Isolated species in the gas phase were treated employing a large cell (20 Å × 21 Å × 22 Å) and the Γ-point only.

We define the average binding energy ($E_b$) per adsorbed species (PyS or S) as follows:

$$E_b^{ads/Au} = \frac{1}{N_{ads}}[E^{ads/Au} - E^{Au} - N_{ads}E^{ads}] \qquad (1)$$

where $N_{ads}$ is the number of adsorbed species in the surface unit cell and $E^{ads/Au}$, $E^{Au}$, and $E^{ads}$ stand for the total energy of the system, the energy of the clean surface, and the energy of the adsorbed radical, S or PyS. The latest is formed when PySH loses the hydrogen atom of the S–H group in the adsorption process. Negative numbers indicate an exothermic adsorption process with respect to the clean surface and the adsorbed phase originated during the adsorption process.

## ■ RESULTS AND DISCUSSION

**XPS Characterization.** Typical high resolution XPS spectra of the S 2p and N 1s PyS SAMs on Au(111) formed by $t = 10$ min immersion time in aqueous 0.1 M NaOH solutions are shown in Figure 1a,b.
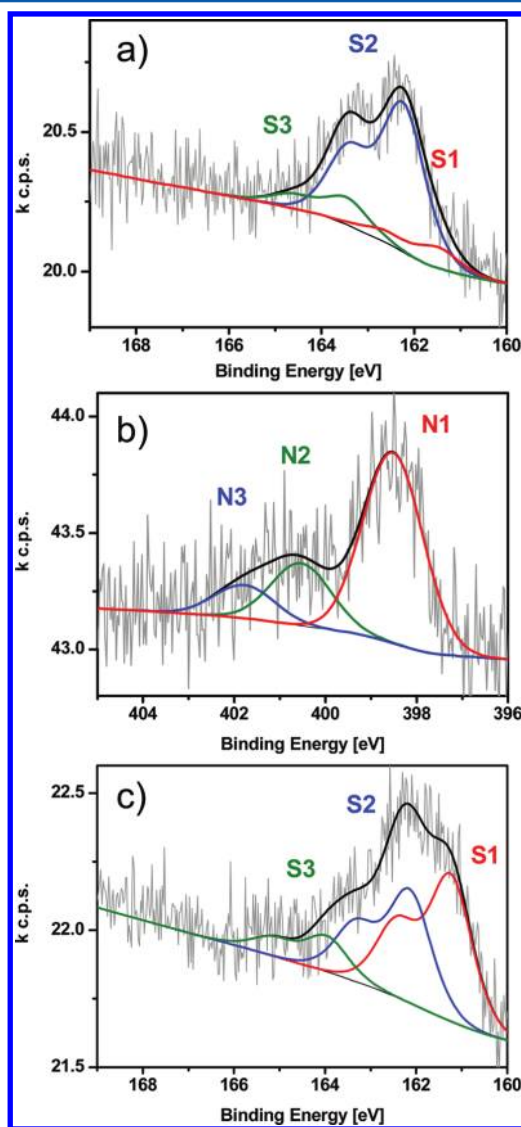


**Figure 1.** High-resolution XPS spectra of the S 2p (a) and N 1s (b) regions for PyS SAMs prepared after immersion of Au(111) substrates in 1 mM PySH aqueous 0.1 M NaOH solutions for $t = 10$ min. (c) S 2p spectra recorded for PyS self-assembled for $t = 10$ min from ethanolic solution.

The S 2p region spectra can be fitted with a main component at S $2p_{3/2}$ BE = 162.3 eV (S2), which has been assigned to the formation of a thiolate bond on Au(111), and two smaller components at S $2p_{3/2}$ BE = 161.4 eV (S1), which correspond to atomic S, and at 163.4 eV (S3), which could be assigned either to unbonded PySH, dypyridyl disulfides, or dipyridyl sulfides.[41]

The S1 and S3 signals represent 8.9% and 14.3% of the S species, respectively; i.e., thiolates (76.8%) are the dominant species at the Au(111) surface (Figure 1a). These results also confirm that the PyS is chemisorbed by the S atom from the alkaline solution.[42] On the other hand, the Au 4f region can be fitted with a single component with Au $4f_{7/2}$ BE = 84.0 eV, which corresponds to metallic gold, with no contribution from oxidized gold. We have also recorded the N 1s signal (Figure 1b). We can fit the spectrum with a main component located at 398.5 eV (N1) and two smaller ones at 400.5 eV (20%) (N2) and 401.8 eV (12%) (N3). The N1, N2 and N3 signals could be assigned to N atoms of the pyridine ring deprotonated (398.5 eV)[43] and protonated in different interaction extent (400.5 and 401.8 eV).[12,43] In fact, the complex N 1s emission has been interpreted considering different degrees of H-acceptance and protonation of the pyridine moieties in the SAM from adsorbed water.[44]

From Figure 1a,b we can perform some interesting conclusions. First, the S/Au ratio is larger than that found for a HT SAM used as reference in this work. In fact, the $S_{(total)}$/Au ratio after PyS self-assembly represents a surface coverage $\theta \approx 0.40$ instead of $\theta = 0.33$ found for the HT SAM. This excess results from the contribution of atomic sulfur and unbounded PySH species (or dipyridyl disulfide or dipyridyl sulfide). Second, from the S2/Au intensity ratio the surface coverage by thiolates results in $\theta = 0.33$, a figure close to the value expected for dense thiol monolayers on Au(111). However, it should be noted that adsorbed S (S1 signal) is usually accompanied by similar amounts of polysulfides species that also originate an S 2p signal at 162.3 eV, thus overlapping with the S2 thiolate component. It means that the real surface coverage by the PyS species should be somewhat smaller than that corresponding to a close packed thiol monolayer in $(\sqrt{3} \times \sqrt{3})$-$R30°$ lattice. An estimation of the real PyS coverage can be made by electrochemical measurements as discussed in the next section. On the other hand, we have observed that the total N/S intensity ratio is $\approx 1$, in good agreement with the molecular PySH formula. However, the existence of atomic sulfur (S1 signal $\approx 10\%$) strongly suggests the presence of an amount of richer N species such as dipyridyl sulfides that could compensate the atomic S to give the total N/S ratio is $\approx 1$. This is supported by the S3 component ($\approx 14\%$) in the SAM that could be originated by these species.

Therefore, our picture derived from the XPS data of PyS adsorbed from aqueous 0.1 M NaOH solutions for 10 min involves a large amount of PyS chemisorbed to the Au surface by a thiolate bond including a small amount of polysulfides (76%), some amounts of dipyridyl sulfides, dipyridyl disulfides, and unbonded PySH (14%), and adsorbed atomic sulfur atoms (10%).

On the other hand, the XPS data changes markedly when PySH is self-assembled from ethanolic solutions for the same immersion time $t = 10$ min (Figure 1c). In this case the S 2p core level region shows that the adsorbed atomic S component (S1) becomes dominant (53.5%), followed by a 33.5% of the S2 component and a 13% of the S3 signal. The S1 + S2

components represent a S coverage $\approx 0.5$. This kind of spectra is typical of a Au(111) surface covered by a monolayer of adsorbed S (S coverage $\approx 0.66$).[6] The dominant presence of S molecules in the Au(111) surface is consistent with the total S/N ratio $\approx 3$ rather than 1 expected for the intact molecules. Therefore, the S2 signal arises mainly from polysulfide species and not from thiolate–Au bonds as a small amount of PyS seems to be present on the Au(111) surface. In a similar way, the small S3 can be assigned to some amount of elemental S as already reported for S on Au(111).[8]

**Electrochemical Data.** Reductive desorption curves (RDC) have been used to estimate the surface coverage by thiolates and S on the Au(111) surface. In fact, desorption of S species originates broad current peaks located at $-0.95$ V (S from terraces) and $-1.15$ V (S from steps)[45] while desorption of PyS results in a peak located at $\approx -0.6$ V.[46]

In Figure 2, a typical RDC recorded at 0.05 V s$^{-1}$ in 0.1 M NaOH is shown for PyS prepared on Au(111) by immersion of
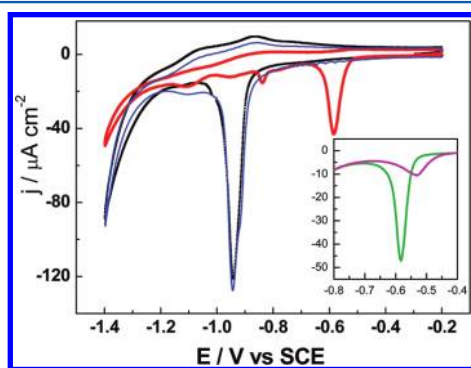


**Figure 2.** First RDC of PyS SAMs on Au(111) prepared by immersion for different times and solvents: (red) 10 min in aqueous 0.1 M NaOH solutions, (black) 24 h in aqueous 0.1 M NaOH, solutions, (blue) 10 min ethanol. Scan rate: 0.05 V s$^{-1}$. Electrolyte: 0.1 M NaOH. Note that black and blue lines are superimposed in the cathodic peak. Inset: first (green) and second (pink) consecutive RDC of PyS SAMs on Au(111) prepared by immersion for 10 min in aqueous 0.1 M NaOH solutions.

the clean substrate in aqueous 0.1 M NaOH for $t = 10$ min (red line). This RDC corresponds to a sample with the S 2p and N 1s spectra shown in Figure 1a,b. The sharp reductive desorption peak found at $-0.58 \pm 0.01$ V (vs SCE) has been interpreted by the reaction[21,46]

$$\text{PyS--Au} + e^- = \text{PyS}^- + \text{Au} \qquad (2)$$
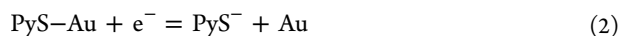
The peak charge density is $q = 45 \pm 4\ \mu\text{C cm}^{-2}$, which corresponds to a surface coverage $\theta \approx 0.20$ taking into account that a complete thiol monolayer in $(\sqrt{3} \times \sqrt{3})$-$R30°$ lattice ($\theta = 0.33$) should involve 75 $\mu$C cm$^{-2}$. This coverage is close to that expected for the $(5 \times \sqrt{3})$ and $(7 \times \sqrt{3})$ lattices on Au(111) observed by in situ STM in acid solutions containing PySH.[12] The second consecutive RDC (inset in Figure 2) shows that the charge involved in the main peak at $-0.58$ V markedly decreases while the peak potential shifts slightly in the positive direction indicating that only a small amount of PyS can be reabsorbed. This fact results from the rapid diffusion of the molecules away from the Au surface favored by the solubility of the PyS molecules in the electrolyte.

In addition to the main peak at $-0.58$ V (related to desorption of the PyS) other smaller peaks appear at $-0.88$, $-0.95$, and $-1.15$ V. As mentioned above, these peaks can be

related to desorption of S from terraces ($-0.88$ and $-0.95$ V) and from steps ($-1.15$ V) according to the reaction[45]

$$\text{H}_2\text{O} + \text{S--Au} + 2e^- = \text{SH}^- + \text{OH}^- + \text{Au} \qquad (3)$$
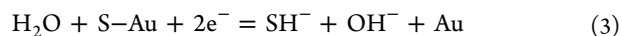
The total charge density involved in these small peaks is $q = 10 \pm 4\ \mu\text{C cm}^{-2}$ that should correspond to an S coverage $\theta \approx 0.02$ considering that desorption of a complete S monolayer from a $(\sqrt{3} \times \sqrt{3})$-$R30°$ lattice according to reaction 3 involves $q = 150\ \mu\text{C cm}^{-2}$. From the electrochemical data the sulfide/thiolate ratio results in $\approx 0.1$, close to that derived from the XPS data (10%).

The increase in the immersion time from $t = 10$ min to 24 h in the aqueous 0.1 M NaOH solution changes drastically the electrochemical data as shown in Figure 2 (black line). First, the large peak located at $-0.58$ V (red curve) disappears, and the small ones located at $\approx -0.88$ and $-0.95$ V merge into a single and broad peak at $-0.95$ V involving a charge density $q = 140 \pm 4\ \mu\text{C cm}^{-2}$. The position and charge density of this large peak are typical of a Au(111) substrate covered by a monolayer of adsorbed S. Also, the small peak at $-1.15$ V, which has been previously related to desorption of S from steps edges,[45] is visible under these self-assembly conditions. We have interpreted these electrochemical results considering the complete disappearance of the PyS moieties that have been replaced or transformed by/into an adsorbed S monolayer. A similar RDC than that shown in Figure 2 for PyS SAMs prepared in aqueous 0.1 M NaOH for 24 h is recorded for the self-assembly from ethanolic solutions, irrespective of the immersion time (Figure 2, blue line). In fact, the broad peak at $-0.95$ V involving a similar $q$ value indicates the presence of S monolayer, in agreement with the XPS data shown in Figure 1c.

Our results demonstrate that PySH adsorption on Au(111) involves the formation of a diluted self-assembled monolayer that is transformed or replaced by a complex atomic S + polysulfide layer by increasing the immersion time. This process is slow in aqueous solutions and very fast in ethanol.

**STM Imaging.** STM images taken after Au(111) immersion in the PySH containing either aqueous 0.1 M NaOH or ethanol for 10 min are shown in Figures 3a and 3b, respectively. The Au surface after immersion in aqueous 0.1 M NaOH shows a large
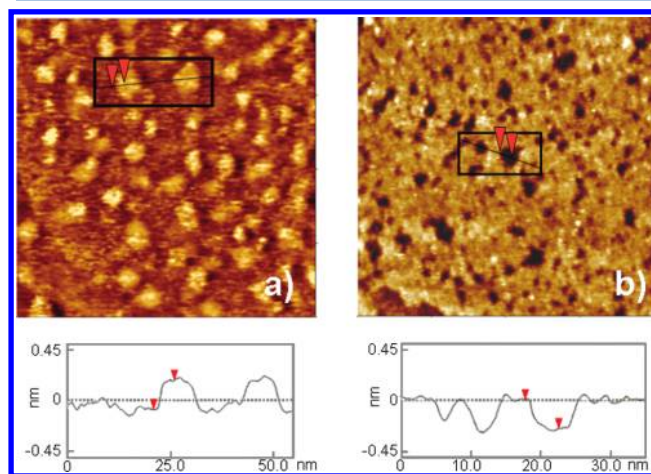


**Figure 3.** 100 × 100 nm$^2$ top view STM images (raw data) of Au substrates in contact for 10 min in (a) 1 mM PySH aqueous 0.1 M NaOH solution and (b) 1 mM PySH ethanolic solution. The lower panels show typical cross sections of the (a) islands and (b) pits obtained in the aqueous and ethanolic solutions, respectively.

**Table 1. Binding Energies, Structural Data, and Bader Charges for S and Au Atoms in the Different PyS SAMs Lattices on Au(111) (Nonitalic Data with vdW, Italic without vdW)**

| unit cell | site | $E_b$/eV | $d_{S-Au}$/Å | $d_{S-C}$/Å | $\alpha$/deg | Bader charge/$e$ S | Bader charge/$e$ Au$_{top layer}^{average}$ |
|---|---|---|---|---|---|---|---|
| $(7 \times \sqrt{3})$ PyS | b-fcc | | 2.48; 2.48; 3.25 | 1.78 | 37 | −0.12 | |
| | *b-fcc* | | *2.51; 2.51; 3.15* | *1.78* | *36* | *−0.07* | |
| | b-fcc | −2.47 | 2.50; 2.42; 3.16 | 1.78 | 36 | −0.10 | +0.01 |
| | *b-fcc* | *−1.64* | *2.51; 2.49; 3.05* | *1.78* | *36* | *−0.04* | *+0.02* |
| | b | | 2.47; 2.48; 3.68 | 1.79 | 31 | −0.15 | |
| | *b-fcc* | | *2.44; 2.48; 2.95* | *1.78* | *32* | *−0.15* | |
| $(\sqrt{3} \times 3)$-$R30°$ PyS | b-fcc | −2.44 | 2.49; 2.49; 3.09 | 1.78 | 31 | −0.15 | +0.04 |
| | *b-fcc* | *−1.41* | *2.49; 2.48; 3.08* | *1.78* | *31* | *−0.11* | *+0.04* |
| $(\sqrt{3} \times 3)$-$R30°$ S | fcc | −3.98 | 2.41; 2.41; 2.41 | - | - | −0.3 | +0.1 |
| | *fcc* | *−3.56* | *2.41; 2.41; 2.42* | *-* | *-* | *−0.25* | *+0.12* |

number of islands nanometer in size and one Au atom in height (Figure 3a). Therefore, they can be assigned to Au islands. In contrast, the Au surface after immersion in ethanol exhibits only a large number of pits also one Au atom in depth (Figure 3b). The differences in topography seem to correlate to the different surface chemistry that these samples have: mostly a PyS SAM on Au after self-assembly in PySH containing aqueous electrolyte and an adsorbed S monolayer on Au for the self-assembly from the PySH containing ethanolic solution. In fact, island formation has been reported for PySH SAMs and other aromatic thiols in aqueous solutions[9] while pits are found for aliphatic thiols and sulfur.[6] While the presence of pits in PyS SAMs prepared in ethanol has been related to extensive etching of the Au(111) surface by the formation of soluble PyS–Au(I)–SPy complexes,[29] the presence of Au islands in PyS SAMs has been related to the strong intermolecular forces among the aromatic rings.[9]

**DFT Calculations.** The molecule−substrate and molecule−molecule interactions have been considered as the main factors involved in the stability of the thiol SAMs and also in the reconstruction of the substrate yielding vacancies or islands. We have used the DFT calculations for the $7 \times \sqrt{3}$ PyS and $(\sqrt{3} \times \sqrt{3})$-$R30°$ S lattices, which are consistent with our experimental surface coverage for these species, to estimate the PyS−Au and S−Au interactions with and without taking into account the long-range dispersion corrections (vdW) (Table 1). We have also estimated these quantities for a hypothetical $(\sqrt{3} \times \sqrt{3})$-$R30°$ PyS lattice, although it has been not experimentally observed yet. The optimized structures are shown in Figure 4. Table 1 also include different structural parameters of these lattices on the Au(111) surface.

First, we note that the binding energy of the $7 \times \sqrt{3}$ PyS lattice without van der Waals interactions is $E_b$ = −1.64 eV, a value that results in well agreement with that estimated previously[23] for the same lattice, while the $(\sqrt{3} \times \sqrt{3})$-$R30°$ PyS has a slightly smaller $E_b$ value. Both $E_b$ values are markedly lower to that found for methanethiolate in a $(\sqrt{3} \times \sqrt{3})$-$R30°$ lattice on the unreconstructed Au(111) ($E_b$ = −1.82 eV)[6] and much lower than that estimated for S in a $(\sqrt{3} \times \sqrt{3})$-$R30°$ ($E_b$ = −3.56 eV) (Table 1) and polysulfide (S octomers) species ($E_b$ = −3.5 eV).[47]

However, when van der Waals interactions are included, the $E_b$ values of the PyS lattices markedly increase although they still remain much smaller than the adsorbed sulfur. Note that the $E_b$ values including van der Waals interactions are larger than that estimated for hexanethiolate on unreconstructed Au(111) ($E_b \approx$ −2.08 eV) and close to those expected for these
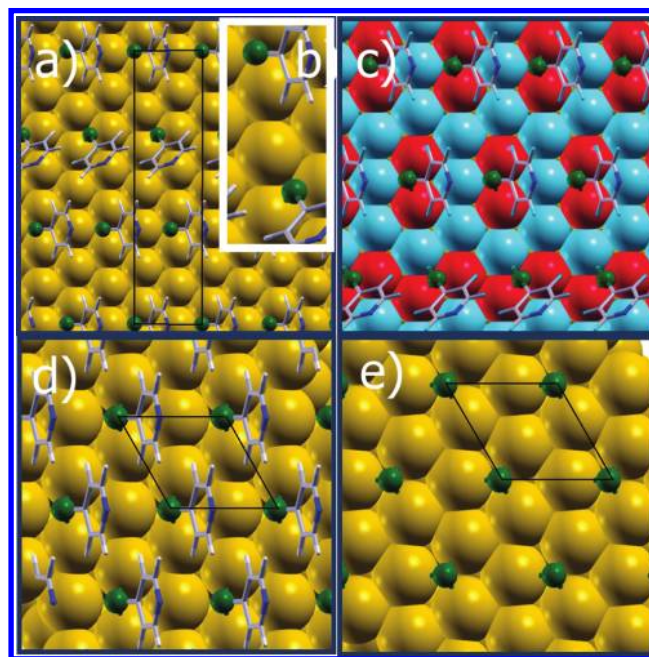


**Figure 4.** Optimized surface structures: (a) $(7 \times \sqrt{3})$ PyS, (b) details of the $(7 \times \sqrt{3})$ PyS lattice showing the PyS adsorption on b-fcc and b-sites, (c) Bader charge of the topmost Au atoms in the $(7 \times \sqrt{3})$ PyS lattice; red: positive, blue: negative, (d) $(\sqrt{3} \times 3)$-$R30°$ PyS, (e) $(\sqrt{3} \times 3)$-$R30°$ S. Green: S, gray: C, white: H, blue: N. The corresponding units cell are drawn on the figures.

SAMs arranged in the most stable adatom-containing model on reconstructed Au(111) surfaces ($E_b \approx$ −2.6 eV).[6]

It should be also noted that the tilt angle (with respect to the substrate normal) for the PyS lattices without and with vdW interactions is ≈30° as estimated for other aromatic and aliphatic thiols on Au(111).[6]

We have also performed a Bader charge analysis (Table 1). In all cases we observe that S atoms in the SAMs are negatively charged. On the other hand, topmost Au atoms show a more complex behavior. In the case of the $(7 \times \sqrt{3})$ lattice the Au atoms bonded to S have positive charges (red atoms in Figure 4c) while the other are negatively charged (blue atoms in Figure 4c). The average charge per Au atom in the topmost layer is nearly zero (+0.01). This result contrasts to that observed for the hypothetical $(\sqrt{3} \times \sqrt{3})$-$R30°$ PyS lattice where all topmost Au atoms are positively charged (average charge per Au atom = +0.04) very close to that calculated for methanethiolate in the same lattice (+0.05).[6] On the other

hand, the topmost Au atoms in the $(\sqrt{3} \times \sqrt{3})$-$R30°$ S lattice have the largest average positive charge (+0.1).

The charge distribution on the topmost Au atoms for the PyS SAM resembles closely that found for 6-mercaptopurine, other heterocyclic N-containing molecule that also exhibits a diluted thiol lattice and no evidence of pit formation.[48]

Several conclusions can be drawn from these calculations. First, it is evident that the interactions among aromatic rings in the SAMs are very important to stabilize the SAM and cannot be neglected as it has been done previously.[23] Second, the easier electrochemical desorption of the PyS SAM (−0.6 V) in relation to HT SAM (−0.9 V) cannot be understood in terms of $E_b$. Indeed, it should reflect the higher solubility of PyS$^-$ than alkylthiolates in the aqueous NaOH solutions (see inset in Figure 2), a fact that favors the PyS desorption from the SAM.[49] The third conclusion refers to the strong interaction of the S species with the Au atoms (Table 1) that can explain the progressive replacement of the adsorbed PyS species for the S ones, irrespective of the S source. Finally, one could speculate that the repulsion originated in the positive charge accumulated at the topmost Au layer should be responsible of pit formation by ejection of Au atoms[50,51] as no pits are observed for PyS and 6-mercaptopurine (negative and positive Au atoms), and strong pitting is observed for alkanethiols and S (all positive Au atoms). In fact, it has been proposed that the charge separation at the thiol−Au interface induced by alkanethiol adsorption produces surface stress due to the accumulation of positive charges at the substrate surface. This process could result in Au−Au bond elongation and Au atom ejection yielding etch pits.[51,52] A uniform distribution of positive charges at the Au surface seems to be associated with the formation of the most dense thiolate lattices such as $(\sqrt{3} \times \sqrt{3})$-$R30°$ or c(4 × 2). However, the fact that Au island formation is induced by PySH and other aromatic thiols[9] adsorption but not in 6-mercaptopurine remains to be explained.

**Complex Chemistry of the PySH.** At this stage different reactions can originate the adsorbed atomic S which, in different amounts depending on the solvent and self-assembly time, is present on the Au(111) surface. The first one (M1) could be the simple cleavage of the C−S bond at the Au surface yielding adsorbed S and Py species.[53] In fact, C−S bond scission has been proposed for short alkanethiols[14] and recently for a thioglucose SAM.[54] The second possibility (M2) is the addition of a PySH molecule after cleavage of the SH moiety at the N atom of the adsorbed PyS, a reaction that could produce sulfides.[26] The free sulfides can readsorb displacing the PyS and Py−PyS moieties from the Au surface. The third reaction (M3) involves PySH adsorption at defects yielding PyS−Au(0)−SPy units and, as a side reaction, Py−S−Py and S.[29] Also, in the presence of O$_2$ and ethanol the PyS−Au(0)−SPy species could form soluble PyS−Au(I)−SPy complexes, resulting in massive Au etching explaining the presence of pits. Finally, the fourth possibility (M4) is the replacement of the PyS species by traces of atomic S present in the PySH chemical, and accordingly, in the working solutions.[21] In the next sections we will try to unify our results and the precedent models in order to explain the complex path that takes place in PyS SAMs degradation.

**Surface Reactions of Adsorbed PyS on Au(111).** In order to elucidate if the PySH species or S contaminants in solution plays a key role in sulfidization, we have self-assembled PySH in the aqueous 0.1 M NaOH solutions for 10 min, a procedure that, as shown in Figures 1 and 2, results mostly in the formation of PyS adsorbates as thiolates and then immersed

these Au substrates in water or ethanol for 24 h. When this procedure is applied using water as solvent, the RDCs show a similar amount of sulfide and some decrease in the amount of PyS with respect to the initial sample (Figure 5). The fact that
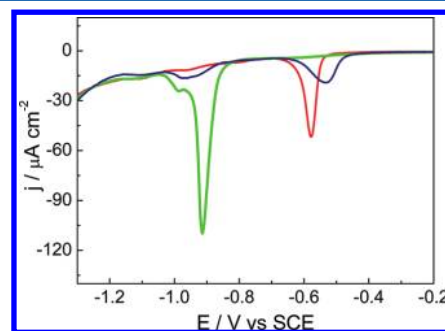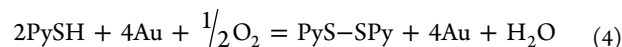


**Figure 5.** RDCs of PyS SAMs on Au(111) prepared by immersion for 10 min in aqueous 0.1 M NaOH solutions (red) and then immersed for 24 h in water (blue) or for 24 h in ethanol (green). Scan rate: 0.05 V s$^{-1}$. Electrolyte: 0.1 M NaOH.
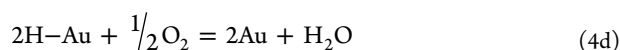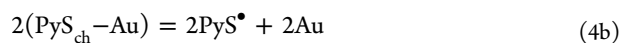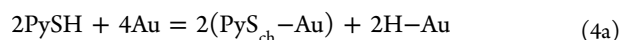
the amount of atomic sulfur does not show a significant increase during immersion in water implies that the atomic sulfur is not efficiently formed from the adsorbed PyS species in this solvent. The decrease in the amount of PyS with time is consistent with some oxidation of the thiol molecules to physisorbed disulfide species as already reported in the presence of light and O$_2$.[4] In contrast, the amount of atomic sulfur markedly increases with respect to that initially present on the surface when PyS SAMs on Au(111) are immersed for 24 h in ethanol. The charge density related to atomic sulfur increases from $q = 10\ \mu C\ cm^{-2}$ to $q = 100\ \mu C\ cm^{-2}$ that implies an increase in the S surface coverage from $\theta = 0.02$ to $\theta = 0.22$, and more importantly, the desorption peak of the PyS SAM completely disappears ($\theta = 0.2 \Rightarrow \theta = 0$). It means that the previously adsorbed PyS species completely transform into atomic S in ethanol. The observation of this surface process taking place is an interesting result because it allows us to discard the need of additional PySH molecules from the solution or S species as impurities for sulfidization and that this surface reaction is markedly enhanced in ethanol. Therefore, processes M2 and M4, being also possible, are not really needed to produce sulfidization of the Au(111).

The contribution of other reactions involving PySH or traces of atomic S in solution to sulfidization was demonstrated by reducing the immersion time of the preformed PyS SAM in ethanol from 24 h to 10 min. In this case the SAM degradation is not significant, indicating that the surface reaction is a relatively slow process. Thus, the sulfidization observed after self-assembly in PySH containing ethanolic solutions for 10 min involves other reactions that take place in parallel to the surface process. The fact that these reactions are slow in 0.1 M NaOH solutions can be explained in terms of the higher solubility of the S-containing species in ethanol that in aqueous solutions.
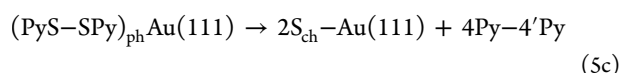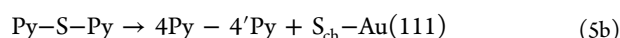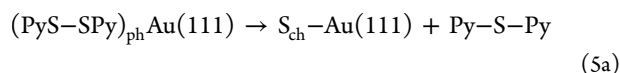
**A Possible Mechanism for Au Sulfidization by Surface Reactions.** In principle, our results for the PyS SAM degradation in contact with both pure ethanol or water solvents could be explained by the following reactions:

$$2\text{PySH} + 4\text{Au} + \tfrac{1}{2}\text{O}_2 = \text{PyS−SPy} + 4\text{Au} + \text{H}_2\text{O} \quad (4)$$

with the following mechanism

$$2PySH + 4Au = 2(PyS_{ch}-Au) + 2H-Au \quad (4a)$$

$$2(PyS_{ch}-Au) = 2PyS^{\bullet} + 2Au \quad (4b)$$

$$2PyS^{\bullet} = PyS-SPy_{ph} \quad (4c)$$

$$2H-Au + \tfrac{1}{2}O_2 = 2Au + H_2O \quad (4d)$$

where the ch and ph subindexes in eqs 4a,4c stand for chemisorbed and physisorbed species. We propose that physisorbed dipyridyl disulfide reacts yielding dipyridyl sulfide and atomic S that is chemisorbed immediately on the Au(111) surface, according to

$$(PyS-SPy)_{ph}Au(111) \rightarrow S_{ch}-Au(111) + Py-S-Py \quad (5a)$$

$$Py-S-Py \rightarrow 4Py - 4'Py + S_{ch}-Au(111) \quad (5b)$$

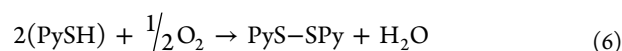$$(PyS-SPy)_{ph}Au(111) \rightarrow 2S_{ch}-Au(111) + 4Py-4'Py \quad (5c)$$

These reactions explain the total sulfidization of the Au surface starting with an adsorbed PyS SAM. Note that reaction 4 is supported by STM images showing that the PyS on Au(111) are dimerized at the sulfur position to form a disulfide.[24,25] On the other hand, it has been found that Py−S−Py species are present in solution when the self-assembly process takes place.[29] Moreover, the photolysis of PyS−SPy under UV radiation has shown to produce $S_8$ species trough the formation of radical species. These previous results reinforce the idea that a more complex mechanism than the simple S−C cleavage (M1) might occur in the sulfidization process of PyS. Also, the shorter S−C distances (0.178 nm, Table 1) in the $7 \times \sqrt{3}$ and $(\sqrt{3} \times \sqrt{3})$-$R30°$ PyS lattices (Table 1) than those found for the PySH molecule in vacuum (0.183 nm) and for chemisorbed alkanethiolates on Au(111) (0.183/0.182 nm depending on the model) suggest a stronger S−C bond. X-ray diffraction measurements of PyS−Au(I)−SPy complexes have shown shorter S−C bonds (0.1736 nm) after the Au−S interaction takes place, accounting for a significant S−C double bond character.[55] The disulfide route seems to be also favored by the weaker S−Au bonding energy in PyS (see Table 1 without vdW interactions) than that found in alkanethiolates.[6]

There are, however two central questions that should be answered: why is this reaction not so important in aliphatic thiols, and why does not this reaction proceed at a significant rate in 0.1 M aqueous solutions NaOH solutions? First, it has been recently reported that aryl thiol derivatives with electron donating and electron withdrawing groups at the para aromatic position of the benzene ring were also efficiently oxidized to the corresponding disulfides as well as other related aromatic thiols while this reaction is very difficult for aliphatic thiols.[56] In addition, as we had shown the Au−S bond seems to be weaker and the S−C bond stronger in the PyS system compare to the aliphatic thiols one. Also, it has been shown that reaction 4 is inhibited in the presence of OH$^-$ ions explaining why we do not observe significant amount of S when the PyS SAM is formed in aqueous 0.1 M NaOH. Also, 4Py−4'Py is more soluble in ethanol than in water, thus favoring the degradation reaction. There is, however, a final issue to be addressed: reaction 4 is catalyzed by gold nanoparticles with sizes smaller than 3.5 nm.[56] We propose that in our system reaction 4 takes place at the edges of the smallest Au islands formed upon PySH
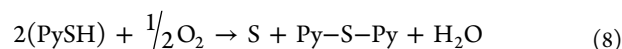
adsorption (Figure 3). Note that organic sulfides do not chemisorb on Au(111) surfaces and cannot be detected in the reductive desorption curves.[15,57]

Finally, it should be noted that our surface reaction pathway explains previous results from STM images. In fact, adsorbed disulfide species (0.2/0.3 nm) were imaged in acid media while S−S distances consistent with thiolates (0.5 nm) were observed in alkaline media.[24] However, in this case a slow SAM disordering assigned to PyS desorption was also observed although no explanation for this process was advanced. In the frame of our model there is an unified pathway: thiolates are oxidized to disulfide which later form S species. This explains the presence of disulfide and the slow disorganization of the PyS lattice which is transformed in adsorbed S. The observation of disulfide or thiolates would depend only on the rate of the degradation process in the different electrolytes.

**A Possible Mechanism for Au Sulfidization from PySH Containing Solutions.** In a previous paper it has been reported that purified solutions of PySH (free of atomic S) also decompose to form sulfide along a few days.[46] Therefore, we propose that in self-assembly from PyS containing solutions the following reactions could also take place

$$2(PySH) + \tfrac{1}{2}O_2 \rightarrow PyS-SPy + H_2O \quad (6)$$

$$PyS-SPy \rightarrow S + Py-S-Py \quad (7)$$

and adding 6 and 7

$$2(PySH) + \tfrac{1}{2}O_2 \rightarrow S + Py-S-Py + H_2O \quad (8)$$

followed by

$$S + Au \rightarrow S_{chem}-Au \quad (9)$$

These reactions should be favored in ethanol (where S is soluble) solutions explaining the rapid sulfidization in this solvent.

The formation of disulfide species from PySH in solution (reaction 6) is supported by previous UV−vis studies of these molecules in different solvents.[58] However, this reaction is relatively slow in aqueous electrolyte. In fact, we performed voltammetric measurements in 1 mM PySH + 0.1 M NaOH electrolyte solution aged during 24 h in ambient conditions. The voltammograms exhibit one anodic and one cathodic current peaks which are characteristic of the adsorption/ desorption of the thiolate at the electrode surface from the PySH present in the electrolyte solution, respectively. The cathodic peak was still centered at −0.58 V, and the charge density for both processes (anodic and cathodic) was also 50 $\mu C/cm^2$. These experiments allows us to confirm that the sulfur peak (centered at −0.95 V) that we observed when the Au surface was incubated in the PySH alkaline solution for 24 h is mainly related to the surface process described by reactions 4a−4d (i.e., no degradation of the PySH solution takes place and S impurities are not present in this solution).

The fact that both sulfidization reactions (surface and solution decomposition) are slow in aqueous alkaline solution explains why it is possible to obtain relatively good PyS SAMs in this electrolyte and short immersion times.

**Etching of the Au(111) Surface.** STM images of the Au(111) surfaces reveal quite different topographies after PySH self-assembly in aqueous 0.1 M NaOH and ethanolic solutions. While the presence of Au islands observed after PySH self-assembly in the aqueous solutions is typical of aromatic thiols

SAMs,[9] the extensive pitting observed in ethanolic solutions has been related to the formation of PyS−Au(I)−SPy complexes where they are soluble (M3).[29] These species are proposed to be formed by the oxidation reaction with molecular oxygen present in the media according to

$$PyS−Au(0)−SPy \rightarrow PyS−Au(I)−SPy_{(sol)} \qquad (10)$$
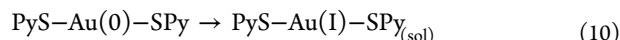
where sol implies species in the solution.

However, we demonstrate in this work that the surface of these samples is completely covered by atomic S. On the other hand, it is well-known that S adsorption induces extensive pitting of the Au surface.[45,47] Therefore, while M3 can not be excluded we consider that the main pitting promoter in this system is the adsorbed atomic S.

## CONCLUSIONS

We have studied the PyS SAM on Au(111) an important platform for many applications in nanoscience and nanotechnology where many aspects remain still unexplained or controversial in the vast literature existing on this system. As mentioned in the Introduction, relevant unsolved issues are the observation of sulfur, disulfide, and thiolate adlayers, depending on the solvent or electrolyte pH, the mechanism of sulfidization, and the strong dependence of surface topography with the solvent. In this context we have demonstrated for the first time that sulfidization takes place not only by solution decomposition, as already suggested, but also by a surface reaction, and that both processes are slow in aqueous alkaline solutions, thus allowing PyS SAM ($\theta \approx 0.2$) formation in this media by using short immersion times. On the other hand, a PyS SAMs prepared in this way is completely decomposed into adsorbed sulfur species by simple immersion in pure ethanol. Thus, the surface reaction allows us preparing Au surfaces with very low amounts of adsorbed S ($\theta < 0.33$), a surface coverage that cannot be reached when the process is made by immersion of the Au substrate in S or polysulfide containing solutions. The previous observations of islands or pits depending on the experimental conditions are now unambiguously explained, since they are clearly associated with the surface chemistry: islands for PyS and pits for S covered Au(111), respectively. Our DFT calculations also give new insights for this system revealing the importance of the van der Waals interactions in stabilizing the PyS SAM on the Au surface, indicating the strengthen of the S−C bond upon adsorption, thus discarding direct S−C bond scission on the Au surface and supporting the mechanism of sulfidization via disulfide formation, the usual pathway for SAM thiol degradation. We propose that the surface-degradation reaction takes place through the formation of a dipyridyl disulfide and catalyzed at the Au island formed upon thiol adsorption which can undergo a further decomposition to atomic S. This mechanism supports the observation of sulfur, disulfide, and thiolate adlayers and the lack of evidence of the denser ($\sqrt{3} \times \sqrt{3}$)-R30° PyS lattice due to the interference of sulfur atoms which have a stronger bonding to the Au surface. Finally, the analysis of the Bader charge derived from the DFT calculations indicates a very small accumulation of positive charge at the topmost Au atoms compared to those estimated for S or alkanethiol lattices, a fact that could explain the absence of pits upon PyS assembly since the surface stress acting at the substrate surface is markedly reduced.

## AUTHOR INFORMATION

**Corresponding Author**

*E-mail rubert@química.unlp.edu.ar; Ph +54 221 4257430; Fax +54 221 4254642.

**Notes**

The authors declare no competing financial interest.

## REFERENCES

(1) Gates, B. D.; Xu, Q.; Stewart, M.; Ryan, D.; Willson, C. G.; Whitesides, G. M. *Chem. Rev.* **2005**, *105*, 1171−1196.

(2) Love, J. C.; Estroff, L. A.; Kriebel, J. K.; Nuzzo, R. G.; Whitesides, G. M. *Chem. Rev.* **2005**, *105*, 1103−1170.

(3) Vericat, C.; Vela, M. E.; Salvarezza, R. C. *Phys. Chem. Chem. Phys.* **2005**, *7*, 3258−3268.

(4) Cortés, E.; Rubert, A. A.; Benitez, G.; Carro, P.; Vela, M. E.; Salvarezza, R. C. *Langmuir* **2009**, *25*, 5661−5666.

(5) Kind, M.; Wöll, C. *Prog. Surf. Sci.* **2009**, *84*, 230−278.

(6) Vericat, C.; Vela, M. E.; Benitez, G.; Carro, P.; Salvarezza, R. C. *Chem. Soc. Rev.* **2010**, *39*, 1805−1834.

(7) Yang, G.; Liu, G.-y. *J. Phys. Chem. B* **2003**, *107*, 8746−8759.

(8) Vericat, C.; Vela, M. E.; Andreasen, G.; Salvarezza, R. C.; Vazquez, L.; Martin-Gago, J. A. *Langmuir* **2001**, *17*, 4919−4924.

(9) Jin, Q.; Rodriguez, J. A.; Li, C. Z.; Darici, Y.; Tao, N. J. *Surf. Sci.* **1999**, *425*, 101−111.

(10) Zangmeister, C. D.; Bertocci, U.; Beauchamp, C. R.; Stafford, G. R. *Electrochim. Acta* **2008**, *53*, 6778−6786.

(11) Zhang, J.; Bilic, A.; Reimers, J. R.; Hush, N. S.; Ulstrup, J. *J. Phys. Chem. B* **2005**, *109*, 15355−15367.

(12) Zhou, W.; Baunach, T.; Ivanova, V.; Kolb, D. M. *Langmuir* **2004**, *20*, 4590−4595.

(13) Wirde, M.; Gelius, U.; Nyholm, L. *Langmuir* **1999**, *15*, 6370−6378.

(14) Cometto, F. P.; Macagno, V. A.; Paredes-Olivera, P.; Patrito, E. M.; Ascolani, H.; Zampieri, G. *J. Phys. Chem. C* **2010**, *114*, 10183−10194.

(15) Zhong, C. J.; Brush, R. C.; Anderegg, J.; Porter, M. D. *Langmuir* **1999**, *15*, 518−525.

(16) Ivanova, V.; Baunach, T.; Kolb, D. M. *Electrochim. Acta* **2005**, *50*, 4283−4288.

(17) Manolova, M.; Ivanova, V.; Kolb, D. M.; Boyen, H. G.; Ziemann, P.; Büttner, M.; Romanyuk, A.; Oelhafen, P. *Surf. Sci.* **2005**, *590*, 146−153.

(18) Nankawa, T.; Suzuki, Y.; Ozaki, T.; Francis, A. J.; Ohnuki, T. *J. Nucl. Sci. Technol.* **2008**, *45*, 251−256.

(19) Urcuyo, R.; Cortés, E.; Rubert, A. A.; Benitez, G.; Montero, M. L.; Tognalli, N. G.; Fainstein, A.; Vela, M. E.; Salvarezza, R. C. *J. Phys. Chem. C* **2011**, *115*, 24707−24717.

(20) Boyen, H.-G.; Ziemann, P.; Wiedwald, U.; Ivanova, V.; Kolb, D. M.; Sakong, S.; Gross, A.; Romanyuk, A.; Buttner, M.; Oelhafen, P. *Nat. Mater.* **2006**, *5*, 394−399.

(21) Yoshimoto, S.; Yoshida, M.; Kobayashi, S.-i.; Nozute, S.; Miyawaki, T.; Hashimoto, Y.; Taniguchi, I. *J. Electroanal. Chem.* **1999**, *473*, 85−92.

(22) Tognalli, N. G.; Cortés, E.; Hernández-Nieves, A. D.; Carro, P.; Usaj, G.; Balseiro, C. A.; Vela, M. E.; Salvarezza, R. C.; Fainstein, A. *ACS Nano* **2011**, *5*, 5433−5443.

(23) Kučera, J.; Gross, A. *Langmuir* **2008**, *24*, 13985−13992.

(24) Wan, L.-J.; Noda, H.; Hara, Y.; Osawa, M. *J. Electroanal. Chem.* **2000**, *489*, 68−75.

(25) Wan, L.-J.; Hara, Y.; Noda, H.; Osawa, M. *J. Phys. Chem. B* **1998**, *102*, 5943−5946.

(26) Gui, J. Y.; Lu, F.; Stern, D. A.; Hubbard, A. T. *J. Electroanal. Chem.* **1990**, *292*, 245−262.

(27) Castner, D. G.; Hinds, K.; Grainger, D. W. *Langmuir* **1996**, *12*, 5083−5086.

(28) Umemura, K.; Fujita, K.; Ishida, T.; Hara, M.; Sasabe, H.; Knoll, W. *Jpn. J. Appl. Phys.* **1998**, *37*, 3620−3625.

(29) Räisänen, M. T.; Kemell, M.; Leskelä, M.; Repo, T. *Inorg. Chem.* **2007**, *46*, 3251−3256.

(30) Park, J.-S.; Vo, A. N.; Barriet, D.; Shon, Y.-S.; Lee, T. R. *Langmuir* **2005**, *21*, 2902−2911.

(31) Daza Millone, M. A.; Hamoudi, H.; Rodríguez, L.; Rubert, A.; Benítez, G. A.; Vela, M. E.; Salvarezza, R. C.; Gayone, J. E.; Sánchez, E. A.; Grizzi, O.; Dablemont, C. l.; Esaulov, V. A. *Langmuir* **2009**, *25*, 12945−12953.

(32) Perdew, J. P.; Chevary, J. A.; Vosko, S. H.; Jackson, K. A.; Pederson, M. R.; Singh, D. J.; Fiolhais, C. *Phys. Rev. B* **1992**, *46*, 6671−6687.

(33) Blöchl, P. E. *Phys. Rev. B* **1994**, *50*, 17953−17979.

(34) Blöchl, P. E.; Margl, P.; Schwarz, K. Ab Initio Molecular Dynamics with the Projector Augmented Wave Method. In *Chemical Applications of Density-Functional Theory*; Laird, B. B., Ross, R. B., Ziegler, T., Eds.; American Chemical Society: Washington, DC, 1996; Vol. *629*, pp 54−69.

(35) Kresse, G.; Joubert, D. *Phys. Rev. B* **1999**, *59*, 1758−1775.

(36) Kresse, G.; Furthmüller, J. *Phys. Rev. B* **1996**, *54*, 11169−11186.

(37) Grimme, S. *J. Comput. Chem.* **2006**, *27*, 1787−1799.

(38) Sławińska, J.; Dabrowski, P.; Zasada, I. *Phys. Rev. B* **2011**, *83*, 245429.

(39) Toyoda, K.; Hamada, I.; Lee, K.; Yanagisawa, S.; Morikawa, Y. *J. Chem. Phys.* **2010**, *132*, 134703.

(40) Monkhorst, H. J.; Pack, J. D. *Phys. Rev. B* **1976**, *13*, 5188−5192.

(41) Lindberg, B. J.; Hamrin, K.; Johansson, G.; Gelius, U.; Fahlman, A.; Nordling, C.; Siegbahn, K. *Phys. Scr.* **1970**, *1*, 286.

(42) Hassan, N. Spectroelectrochemistry of Self-Assembled Monolayers of 2- and 4-Mercaptopyridines. PhD Thesis, Technischen Universität Chemnitz, Chemnitz, 2007.

(43) Silien, C.; Buck, M.; Goretzki, G.; Lahaye, D. e.; Champness, N. R.; Weidner, T.; Zharnikov, M. *Langmuir* **2009**, *25*, 959−967.

(44) Zubavichus, Y.; Zharnikov, M.; Yang, Y.; Fuchs, O.; Umbach, E.; Heske, C.; Ulman, A.; Grunze, M. *Langmuir* **2004**, *20*, 11022−11029.

(45) Vericat, C.; Andreasen, G.; Vela, M. E.; Salvarezza, R. C. *J. Phys. Chem. B* **2000**, *104*, 302−307.

(46) Taniguchi, I.; Yoshimoto, S.; Yoshida, M.; Kobayashi, S.-i.; Miyawaki, T.; Aono, Y.; Sunatsuki, Y.; Taira, H. *Electrochim. Acta* **2000**, *45*, 2843−2853.

(47) Lusteinberg, P. G.; Vericat, C.; Benitez, G. A.; Vela, M. E.; Tognalli, N.; Fainstein, A.; Martiarena, M. L.; Salvarezza, R. C. *J. Phys. Chem. C* **2008**, *112*, 11394−11402.

(48) Pensa, E.; Carro, P.; Rubert, A. A.; Benítez, G.; Vericat, C.; Salvarezza, R. C. *Langmuir* **2010**, *26*, 17068−17074.

(49) Azzaroni, O.; Vela, M. E.; Andreasen, G.; Carro, P.; Salvarezza, R. C. *J. Phys. Chem. B* **2002**, *106*, 12267−12273.

(50) Berger, R.; Delamarche, E.; Lang, H. P.; Gerber, C.; Gimzewski, J. K.; Meyer, E.; Güntherodt, H.-J. *Science* **1997**, *276*, 2021−2024.

(51) Godin, M.; Tabard-Cossa, V.; Miyahara, Y.; Monga, T.; Williams, P. J.; Beaulieu, L. Y.; Lennox, R. B.; Grutter, P. *Nanotechnology* **2010**, *21*, 075501.

(52) Godin, M. Surface Stress, Kinetics, and Structure of Alkanethiol Self-Assembled Monolayers. PhD Thesis, McGill University, Montréal, 2004.

(53) Diógenes, I. C. N.; Nart, F. C.; Temperini, M. L. A.; Moreira, Í. d. S. *Inorg. Chem.* **2001**, *40*, 4884−4889.

(54) Kycia, A. H.; Sek, S.; Su, Z.; Merrill, A. R.; Lipkowski, J. *Langmuir* **2011**, *27*, 13383−13389.

(55) Räisänen, M. T.; Runeberg, N.; Klinga, M.; Nieger, M.; Bolte, M.; Pyykkö, P.; Leskelä, M.; Repo, T. *Inorg. Chem.* **2007**, *46*, 9954−9960.

(56) Corma, A.; Rodenas, T.; Sabater, M. J. *Chem. Sci.* **2012**, *3*, 398−404.

(57) Jung, C.; Dannenberger, O.; Xu, Y.; Buck, M.; Grunze, M. *Langmuir* **1998**, *14*, 1103−1107.

(58) Stoyanov, S.; Petkov, I.; Antonov, L.; Stoyanova, T.; Karagiannidis, P.; Aslanidis, P. *Can. J. Chem.* **1990**, *68*, 1482−1489.